Implantable semiconductor biosensor for continuous in vivo sensing of far-red fluorescent molecules

Thomas O'Sullivan,[1] Elizabeth A. Munro,[2] Natesh Parashurama,[3] Christopher Conca,[4] Sanjiv S. Gambhir,[3] James S. Harris,[1] and Ofer Levi[2,5,*]

[1]*Department of Electrical Engineering, Stanford University, 420 via Palou, Stanford, CA 94305-4075, USA*
[2]*Institute of Biomaterials and Biomedical Engineering, University of Toronto, 164 College Street, Toronto, Ontario, M5S 3G9, Canada*
[3]*Molecular Imaging Program at Stanford, Departments of Radiology and Bioengineering, Bio-X Program, Stanford University, Stanford, CA 94305, USA*
[4]*Chroma Technology Corp., 10 Imtec Lane, Bellow Falls, VT 05101 USA*
[5]*The Edward S. Rogers Sr. Department of Electrical and Computer Engineering, University of Toronto, 10 King's College Road, Toronto, Ontario, M5S 3G4, Canada*
[*]ofer.levi@utoronto.ca

Abstract: We have fabricated miniature implantable fluorescence sensors for continuous fluorescence sensing applications in living subjects. These monolithically integrated GaAs-based sensors incorporate a 675nm vertical-cavity surface-emitting laser (VCSEL), a GaAs PIN photodiode, and a fluorescence emission filter. We demonstrate high detection sensitivity for Cy5.5 far-red dye (50 nanoMolar) in living tissue, limited by the intrinsic background autofluorescence. These low cost, sensitive and scalable sensors are promising for long-term continuous monitoring of molecular dynamics for biomedical studies in freely moving animals.

©2010 Optical Society of America

OCIS codes: (170.3890) Medical optics instrumentation; (170.2520) Fluorescence Microscope; (130.6010) Sensors; (230.5160) Photodetectors; (130.5990) Semiconductors.

References and links

1. T. F. Massoud, and S. S. Gambhir, "Molecular imaging in living subjects: seeing fundamental biological processes in a new light," Genes Dev. **17**(5), 545–580 (2003).
2. M. S. Gee, R. Upadhyay, H. Bergquist, H. Alencar, F. Reynolds, M. Maricevich, R. Weissleder, L. Josephson, and U. Mahmood, "Human breast cancer tumor models: molecular imaging of drug susceptibility and dosing during HER2/neu-targeted therapy," Radiology **248**(3), 925–935 (2008).
3. J. V. Frangioni, "In vivo near-infrared fluorescence imaging," Curr. Opin. Chem. Biol. **7**(5), 626–634 (2003).
4. O. Veiseh, C. Sun, C. Fang, N. Bhattarai, J. Gunn, F. Kievit, K. Du, B. Pullar, D. Lee, R. G. Ellenbogen, J. Olson, and M. Zhang, "Specific targeting of brain tumors with an optical/magnetic resonance imaging nanoprobe across the blood-brain barrier," Cancer Res. **69**(15), 6200–6207 (2009).
5. M. Beiderman, T. Tam, A. Fish, G. A. Jullien, and O. Yadid-Pecht, "A low-light CMOS contact imager with an emission filter for biosensing applications," IEEE Trans. Biomed. Circuit Syst. **2**(3), 193–203 (2008).
6. D. Brennan, J. Justice, B. Corbett, T. McCarthy, and P. Galvin, "Emerging optofluidic technologies for point-of-care genetic analysis systems: a review," Anal. Bioanal. Chem. **395**(3), 621–636 (2009).
7. J. A. Chediak, Z. Luo, J. Seo, N. Cheung, L. P. Lee, and T. D. Sands, "Heterogeneous integration of CdS filters with GaN LEDs for fluorescence detection microsystems," Sens. Actuators A Phys. **111**(1), 1–7 (2004).
8. T. Kamei, and T. Wada, "Contact-lens type of micromachined hydrogenated amorphous Si fluorescence detector coupled with microfluidic electrophoresis devices," Appl. Phys. Lett. **89**(11), 114101 (2006).
9. L. Luan, R. D. Evans, N. M. Jokerst, and R. B. Fair, "Integrated Optical Sensor in a Digital Microfluidic Platform," IEEE Sens. J. **8**(5), 628–635 (2008).
10. L. Martinelli, H. Choumane, K.-N. Ha, G. Sagarzazu, C. Goutel, C. Weisbuch, T. Gacoin, and H. Benisty, "Sensor-integrated fluorescent microarray for ultrahigh sensitivity direct-imaging bioassays: Role of a high rejection of excitation light," Appl. Phys. Lett. **91**(8), 083901–083903 (2007).
11. D. Starikov, F. Benkabou, N. Medelci, and A. Bensaoula, "Integrated multi-wavelength fluorescence sensors," in *Proceedings of IEEE Sensors for Industry Conference*, (Institute of Electrical and Electronics Engineers, 2002), pp. 15–18.
12. E. Thrush, O. Levi, L. J. Cook, J. Deich, A. Kurtz, S. J. Smith, W. E. Moerner, and J. S. Harris, Jr., "Monolithically integrated semiconductor fluorescence sensor for microfluidic applications," Sens. Actuators B Chem. **105**(2), 393–399 (2005).

13. D. C. Ng, T. Tokuda, A. Yamamoto, M. Matsuo, M. Nunoshita, H. Tamura, Y. Ishikawa, S. Shiosaka, and J. Ohta, "On-chip biofluorescence imaging inside a brain tissue phantom using a CMOS image sensor for in vivo brain imaging verification," Sens. Actuators B Chem. **119**(1), 262–274 (2006).
14. B. A. Flusberg, A. Nimmerjahn, E. D. Cocker, E. A. Mukamel, R. P. J. Barretto, T. H. Ko, L. D. Burns, J. C. Jung, and M. J. Schnitzer, "High-speed, miniaturized fluorescence microscopy in freely moving mice," Nat. Methods **5**(11), 935–938 (2008).
15. J. Thomas, A. Ambroise, K. Birchfield, W. Cai, C. Sandmann, S. Singh, K. Weidemaier, and J. B. Pitner, "Long wavelength fluorescence based biosensors for in vivo continuous monitoring of metabolites," Proc. SPIE **6078**, 60781–60789 (2006).
16. O. Levi, T. T. Lee, M. M. Lee, S. J. Smith, and J. S. Harris, "Integrated semiconductor optical sensors for cellular and neural imaging," Appl. Opt. **46**(10), 1881–1889 (2007).
17. M. K. Hibbs-Brenner, K. L. Johnson, and M. Bendett, "VCSEL technology for medical diagnostics and therapeutics," Proc. SPIE **7180**, 71800–71810 (2009).
18. K. D. Choquette, A. Giannopoulos, A. M. Kasten, C. Long, and C. Chen, "2-Dimensional Integrated VCSEL and PiN Photodetector Arrays for a Bidirectional Optical Links," in *IEEE Aerospace Conference*, (Institute of Electrical and Electronics Engineers, 2007), pp. 1–7.
19. G. A. Keeler, D. K. Serkland, K. M. Geib, J. F. Klem, and G. M. Peake, "In situ optical time-domain reflectometry (OTDR) for VCSEL-based communication systems," Proc. SPIE **6132**, 61320A (2006).
20. E. Thrush, O. Levi, W. Ha, G. Carey, L. J. Cook, J. Deich, S. J. Smith, W. E. Moerner, and J. S. Harris, "Integrated semiconductor vertical-cavity surface-emitting lasers and PIN photodetectors for biomedical fluorescence sensing," IEEE J. Quantum Electron. **40**(5), 491–498 (2004).
21. P. Taroni, A. Pifferi, A. Torricelli, D. Comelli, and R. Cubeddu, "In vivo absorption and scattering spectroscopy of biological tissues," Photochem. Photobiol. Sci. **2**(2), 124–129 (2003).
22. B. J. Tromberg, N. Shah, R. Lanning, A. Cerussi, J. Espinoza, T. Pham, L. Svaasand, and J. Butler, "Non-invasive in vivo characterization of breast tumors using photon migration spectroscopy," Neoplasia **2**(1-2), 26–40 (2000).
23. X. Shu, A. Royant, M. Z. Lin, T. A. Aguilera, V. Lev-Ram, P. A. Steinbach, and R. Y. Tsien, "Mammalian expression of infrared fluorescent proteins engineered from a bacterial phytochrome," Science **324**(5928), 804–807 (2009).
24. M. Veiseh, P. Gabikian, S. B. Bahrami, O. Veiseh, M. Zhang, R. C. Hackman, A. C. Ravanpay, M. R. Stroud, Y. Kusuma, S. J. Hansen, D. Kwok, N. M. Munoz, R. W. Sze, W. M. Grady, N. M. Greenberg, R. G. Ellenbogen, and J. M. Olson, "Tumor paint: a chlorotoxin:Cy5.5 bioconjugate for intraoperative visualization of cancer foci," Cancer Res. **67**(14), 6882–6888 (2007).
25. E. M. Sevick-Muraca, and J. C. Rasmussen, "Molecular imaging with optics: primer and case for near-infrared fluorescence techniques in personalized medicine," J. Biomed. Opt. **13**(4), 041303–041316 (2008).
26. T. D. O'Sullivan, E. Munro, A. de la Zerda, N. Parashurama, R. Teed, Z. Walls, O. Levi, S. S. Gambhir, and J. S. Harris, "Implantable optical biosensor for in vivo molecular imaging," Proc. SPIE **7173**, 717309 (2009).
27. M. Dandin, P. Abshire, and E. Smela, "Optical filtering technologies for integrated fluorescence sensors," Lab Chip **7**(8), 955–977 (2007).
28. T. D. O'Sullivan, A. Wechselberger, O. Levi, and J. S. Harris, "Compact Semiconductor Bioluminescence Bio-sensors," in *Frontiers in Optics / Laser Science,* Technical Digest (CD) (Optical Society of America, 2007), paper JMD5.
29. E. Thrush, O. Levi, K. Wang, M. Wistey, J. S. Harris, and S. J. Smith, "Integrated semiconductor fluorescent detection system for biochip and biomedical applications," Proc. SPIE **4626**, 289–297 (2002).
30. W. W. Chow, K. D. Choquette, M. H. Crawford, K. L. Lear, and G. R. Hadley, "Design, fabrication, and performance of infrared and visible vertical-cavity surface-emitting lasers," IEEE J. Quantum Electron. **33**(10), 1810–1824 (1997).
31. J.-H. Kim, D. H. Lim, and G. M. Yang, "Selective etching of AlGaAs/GaAs structures using the solutions of citric acid/H_2O_2 and de-ionized H_2O/buffered oxide etch," J. Vac. Sci. Technol. B **16**(2), 558–560 (1998).
32. K. D. Choquette, K. M. Geib, C. I. H. Ashby, R. D. Twesten, O. Blum, H. Q. Hou, D. M. Follstaedt, B. E. Hammons, D. Mathes, and R. Hull, "Advances in selective wet oxidation of AlGaAs alloys," IEEE J. Sel. Top. Quantum Electron. **3**(3), 916–926 (1997).
33. T. D. O'Sullivan, E. Munro, C. Conca, N. Parashurama, A. de la Zerda, S. S. Gambhir, J. S. Harris, and O. Levi, "Near-Infrared in vivo Fluorescence Sensor with Integrated Dielectric Emission Filter," in *Conference on Lasers and Electro-Optics*, OSA Technical Digest (CD) (Optical Society of America, 2009), paper JWA49.
34. T. Camps, C. Bringer, V. Bardinal, G. Almuneau, C. Amat, E. Daran, J. B. Doucet, P. Dubreuil, and C. Fontaine, "High sensitivity integrated lateral detection in VCSELs," Electron. Lett. **41**(3), 129–131 (2005).

1. Introduction

Molecular imaging is an established technique used to visualize and quantify functional information about biological processes in living systems. As opposed to imaging modalities which mainly provide structural information about subjects, molecular imaging uses functional markers/probes to illuminate specific cellular and sub-cellular pathways and interactions [1]. This information can lead to a greater understanding of biochemistry and pathophysiology at a molecular level, as well as assist in the assessment of new therapeutic

targets and development of new therapies—all in living systems. In vivo fluorescence imaging, in particular, is a molecular imaging technique capable of quantitatively imaging one or more fluorophores at high spatial and temporal resolution with high sensitivity, either at microscopic or macroscopic (whole-body) scales. It has been successfully used, for example, in drug discovery and therapeutic evaluation [2], in studying development and treatment of cancer, in tracking stem cell growth and proliferation in small animals, and is an emerging technique for use in humans [3]. Furthermore, fluorescence imaging can be used to visualize multiple pathways simultaneously through the use of multiple probes, and combined with other imaging modalities to co-register morphological details [4].

While current fluorescent imaging technologies have led to key advances in the understanding of biology and biochemistry, there are limitations. Currently available fluorescence imagers generally use either cooled-CCD cameras or large photomultiplier tubes to sense weak fluorescence emission associated with these experiments. These instruments typically take snapshots, sampling discrete points of continuous, dynamic processes. The animal subject must be physically brought to the instrument periodically for imaging (usually under anesthesia to prevent movement during the imaging). Data cannot be collected continuously for greater than a few hours due to either the anesthesia, or simply the need to attend to the animal's basic needs (food, water, etc.). These large-format imagers also require extra space to support cooling of the detector (necessary for low-noise sensitive operation), a broadband excitation light source, and use optical filters to select an excitation spectral band. One possibility is that miniaturization of the components of the optical imaging system would allow expansion of new approaches to, and applications of in vivo molecular imaging.

Miniature fluorescence sensors (with single or multiple pixel architecture) can be fabricated to match a particular fluorescent probe or a set of probes utilizing semiconductor processing technology and appropriate materials. These sensors are small enough to be implanted in small animals (e.g. rodents) and combined with a wireless telemetry system, enable continuous molecular monitoring in freely-moving animal subjects. Indeed several miniature fluorescence sensing systems have already been developed, but mainly for lab-on-a-chip or microfluidic-based applications [5–12]. These sensors incorporate a light source, such as an LED or a laser, with a nearby photodetector and a fluorescence emission filter. However, there has been limited effort to design or apply these sensors for in vivo applications [13]. Another approach is to use optical fibers and external light sources to sense fluorescence in vivo [14,15] for continuous imaging; however these systems are not completely miniaturized and require the animal to be tethered.

In this work we present the design and fabrication of a monolithically integrated semiconductor (GaAs-based) sensor for far-red to near infrared (NIR) in vivo fluorescence sensing. The sensor incorporates three basic components of a fluorescence system, including: a 675nm vertical-cavity surface-emitting laser (VCSEL) excitation source, a GaAs PIN photodiode, and a fluorescence emission filter. Monolithic integration is important because all components of the device are fabricated using a semiconductor process flow from a single wafer, patterned using photolithography techniques, which allows for arbitrary arrangement of sources and detectors at separation distances on the order of 100µm [16] at minimal cost. The sensor is sensitive to cyanine 5.5 (Cy5.5; GE Healthcare/Amersham)-based NIR fluorescent probes. The importance of the choice of the fluorescence probe will be discussed shortly.

The paper is organized as follows: in Section 2 we discuss our design considerations for an integrated fluorescence sensor specifically for in vivo applications; Section 3 details the epitaxial design and semiconductor fabrication of the sensor; we present the optoelectronic device characteristics in Section 4; and finally in Section 5 we present the in vitro and in vivo sensitivity of the device to Cy5.5 fluorescence.

2. Integrated sensor design for in vivo applications

The layout of a single pixel the sensor is pictured in Fig. 1a, and features two 675nm VCSELs (for redundancy), a GaAs PIN photodiode, a fluorescence emission filter, and elements to limit crosstalk between the light sources and detector. The elements are monolithically

integrated on a single GaAs substrate; a cross-section of the epitaxial layers is shown in Fig. 1b.
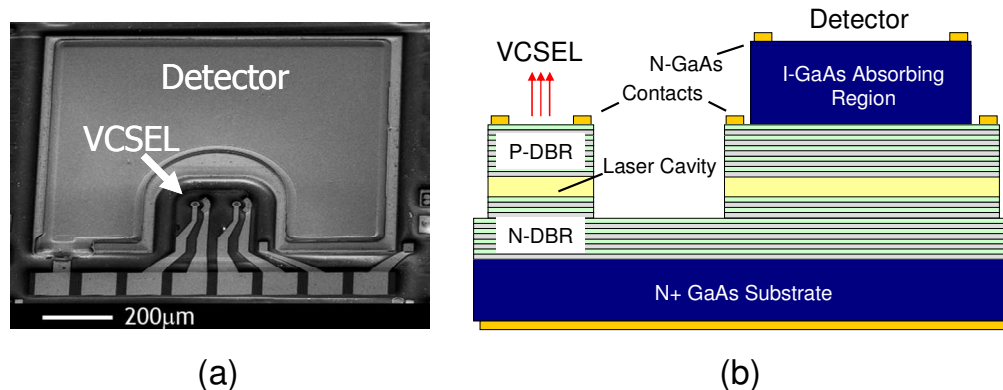

Fig. 1. (a) SEM micrograph of a single-pixel monolithically integrated fluorescence sensor with thin film dielectric fluorescence emission filter and (b) cross-section of the epitaxial layers of the semiconductor-based sensor (not shown to scale).

VCSEL technology, developed extensively for the telecommunications industry, is an excellent light source for integrated fluorescence sensing. VCSELs have been commercialized to emit at 670-980nm, 1300nm and longer wavelengths [17], and can be easily integrated with photodetectors [18–20]. VCSELs emit light normal to the epitaxial layers of a semiconductor wafer (e.g. upward), and thus are well-suited for use in integrated devices for reflectance-based fluorescence sensing. Compared to LEDs, VCSELs emit at higher intensities, allowing for smaller sensor footprints, simpler fabrication designs, and integration of several light sources. VCSELs also exhibit narrower spectral linewidths—typically a full-width half-maxima (FWHM) of less than 0.5nm even when operating as transverse multimode lasers. Narrow excitation spectra allow a good match to a desired fluorescent probe's excitation peak, while maximizing the spectral separation from the nearby emission peak for greater spectral filtration and thus improved fluorescence sensitivity.

For maximum tissue penetration in vivo, we prefer excitation and emission in the far-red to NIR spectral regions (650 to 900nm), where tissue (primarily deoxyhemoglobin, oxyhemoglobin, and water) absorption is minimal. Optical scattering and absorption coefficient values in this spectral region allow sensing in tissue depths of several millimeters [21,22]. Considering the recent development of far-red and NIR fluorescent proteins [23], we choose excitation at 675nm, with detection of NIR fluorescence emission from 700 to 775nm. This choice makes the sensor suitable for a number of far-red and NIR fluorophores including Cy5.5, which has been synthesized into molecular probes for numerous pre-clinical small animal studies [2,24]. However, autofluorescence limits Cy5.5 detection sensitivities in vivo to approximately 50nM [25]. This integrated sensor platform is also appropriate for detecting fluorescent probes with near infrared excitation spectra (>780nm), where lower autofluorescence translates into greater sensitivity in vivo.

During in vivo epi-fluorescence imaging studies, the photodetector collects fluorescence light emitted from within the tissue. The emitted fluorescence light experiences strong attenuation primarily due to scattering ($\mu_s \sim 10$ cm^{-1}). Therefore the photodetector must be sensitive to low photon fluxes ($\sim 10^8$ photons/sec/cm^2/str, based on 675nm nude mouse autofluorescence values), with several orders of linear detection dynamic range. An integrated GaAs PIN photodiode compares favorably to a silicon-based photodetector because intrinsic material properties reduce the dark current, and therefore noise values, by approximately a factor of 10x [16], suitable for low noise un-cooled operation. In addition, we implemented a large-area pixel design (detector area ~0.75 mm^2) in order to collect photons from an approximate 3 x 3 mm tissue cross-section area with a depth of 1-2mm [26], which is suited to

monitor the growth of a tumor. The sensor and collection optics were evaluated and optimized for light collection back from this large tissue volume (cross-section) using a non sequential ray tracing program (ASAP, Breault Research Organization, Tucson, AZ).

An integrated sensor must incorporate methods to prevent the un-desired excitation light from being absorbed by the photodetector. In this miniature architecture, the excitation source and photodetector are placed in close proximity which contributes to considerable crosstalk. Sensors designed for in vivo applications must furthermore cope with the large quantity of excitation light backscattered by the tissue. This background signal will vary in time because the tissue may move with respect to the sensor due to subject mobility, respiration, or cardiovascular dynamics. This imposes additional challenges compared to in vitro sensing applications where the sample chamber and volume is well-controlled and fixed. Indeed the back-scattered excitation light can be several orders of magnitude higher than the fluorescence emission. Excitation light blocking, in the form of interference-based reflection filters, absorption-based filters, or light-guiding techniques, have been used in integrated fluorescence sensors [27]. Thin-film interference-based filters [12] and some absorption-based filters [5,7,10] deposition techniques, are compatible with the robust processing techniques used to fabricate semiconductor devices. The sensors presented here include a monolithically-integrated dielectric-based notch filter, designed and deposited by Chroma Technology, Inc (Bellows Falls, VT) combined with an absorption-based filter. The pixel architecture also includes optical blocking layers to prevent light from leaking around the monolithic filter, or through the sides of the photodetector mesa.

3. Sensor fabrication

3.1 Epitaxial Design

The monolithic integration of the GaAs-based VCSEL/PIN is fabricated from an epitaxial structure which can be designed with either the GaAs detector absorption region (~2µm thick) located above or below the VCSEL layers. This choice is important as it can greatly influence the overall performance of the device, as well as the complexity of the semiconductor device growth and process flow. The primary factors to consider in choosing the location of the detector with respect to the laser epitaxial layers are the quality of the epitaxial layers and the potential optical crosstalk between the laser and the detector. We have previously shown that the detector dark current in GaAs etched-mesa photodiodes is limited by carrier generation due to the surface defect states of the thick intrinsic absorption region, and not due to bulk crystal defects [28,29]. Therefore, the performance of the detector, specifically dark current, is not expected to be highly dependent on quality of the bulk PIN layer growth. But we do desire a high-quality VCSEL layer structure because of the challenge to achieve lasing in the shorter-wavelength AlGaInP-based VCSELs [30]. Therefore, in this work, the VCSEL epitaxial layers are grown first, followed by a PIN photodetector layer growth, in a single recipe by metallo-organic chemical vapor deposition (MOVCD) technique. Our measurements have confirmed that the GaAs photodetector dark current values were not affected by the presence of the underlying VCSEL structure.

3.2 Semiconductor Processing

A schematic of the process flow appears in Fig. 2. The entire process consists of ten, direct-contact photolithography mask steps, which include the fabrication of an oxide-confined VCSEL first, followed by the fabrication of a mesa detector and contact deposition. Fabricating the detector after the VCSEL allows us to achieve extremely low dark current. We do not subject the detector sidewalls to the high-temperature wet oxidation step used to define the oxide aperture of the VCSEL since the detector dark current is determined primarily by the quality of its sidewalls.

The detector epitaxial layers are located above the VCSEL and an initial fabrication step is required to etch away the detector material above the VCSEL. A 100nm-thick $Al_{0.92}Ga_{0.08}As$ layer is used as an etch-stop layer between the thick intrinsic absorption region and the top

VCSEL (and bottom detector) P contact layer. Electron cyclotron resonance-reactive ion etching (ECR-RIE) technique is used to etch away a majority of the detector region above the top VCSEL contact layer, followed by selective wet etches. After ECR-RIE dry etching, a citric acid: 30% H_2O_2 (12:1) wet etch mixture is used to remove the remainder of the detector active (GaAs) layer. This wet etch process selectively stops on the $Al_{0.92}Ga_{0.08}As$ layer. A buffered oxide etch solution (6:1 BOE):DI water (1:15) is used to remove the $Al_{0.92}Ga_{0.08}As$ layer [31] (noticeable by color change – reverting to a mirror-like surface) to completely expose the top P-GaAs VCSEL contact layer. Top side Pt/Ti/Pt/Au P VCSEL metal contacts are defined with a bilayer liftoff process and subsequent metal deposition by electron beam evaporation (Fig. 2b). All the subsequent contacts are defined and deposited with the same method. The VCSEL mesa is defined and etched via ECR-RIE, passing through the quantum wells (QW) active layer and into the first few pairs of the bottom DBR. The etch depth for the VCSEL mesa is a critical parameter, and will influence the current confinement profile, heating effects, and VCSEL QW temperature. This etch depth was monitored via *in situ* optical reflectometry. The current/optical aperture is formed by a selective wet oxidation process [32] in a 440C wet oxidation furnace with nitrogen atmosphere. A global back side Au/Ge/Ni/Au N contact is deposited (Fig. 2c) and contacts thermally annealed. At this point, we can test the VCSELs before proceeding to detector fabrication.
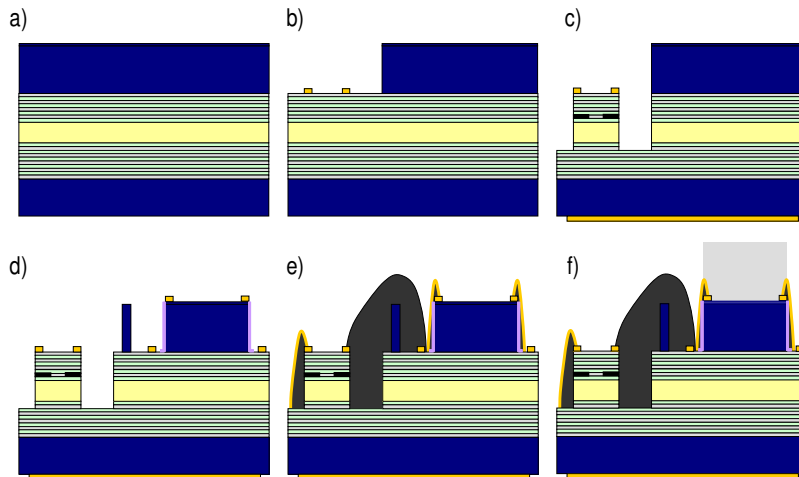

Fig. 2. Fabrication process flow of the integrated VCSEL/PIN photodetector substrate (a) includes: b) removal of the detector layers above the VCSEL and depositing top VCSEL P contacts; c) etching of the VCSEL mesa, oxidation, and deposition of a backside contact; d) depositing a top N PIN detector contact, etching the detector, passivation, and depositing a bottom P PIN contact; e) formation of hard 3D photoresist microstructures for contact vias and optical blocking; and f) lift-off of a thin-film dielectric fluorescence filter.

Detector fabrication begins by evaporating the top Au/Ge/NiAu contact and etching the large detector mesa (Fig. 2d). In a process similar to the removal of the detector layers from above the VCSEL, a combination of dry and selective wet etch processes is used to etch the detector mesa. The etch process is designed to reach the p-GaAs layer below the detector active region, and use it as a bottom detector contact layer. At the same time, a barrier is created as a "wall" between the laser and the detector mesa structures (Fig. 2d) to further reduce optical crosstalk between these devices. The selective wet etch process described above cleans up the plasma etch damage which affects the detector sidewall quality. After the selective wet etch step, the wafer is immediately transferred into a plasma-enhanced chemical vapor deposition (PECVD) chamber for deposition of a 150-200nm silicon nitride passivation layer on the detector sidewalls. The silicon nitride is patterned with photolithography and a subsequent SF_6/O_2 plasma etch to retain the layer on the detector sidewalls and a contact pad region (for gold wire bonding) while removing the layer from all other sensor regions. We

discuss the effectiveness of the sidewall cleanup and passivation in the next section. The detector fabrication is complete with the deposition of a bottom Pt/Ti/Pt/Au P contact on the same plane used as a VCSEL top P contact layer. At this point, we can test the detector performance by evaluating dark current and light responsivity values before proceeding to finish the integration.

The next series of steps define the electrical contact vias to the VCSEL and detector, as well as provide optical light blocking layer between the two. We modify a process previously described by Thrush et al [20] to create cured 3D photoresist microstructures around the VCSEL and detector mesa structures. The sides of the detector are covered with the cured photoresist and over-coated with a Ti/Au metal layer as an opaque optical blocking layer (Fig. 2e). Note that for complete isolation of the VCSEL and adjacent detector, it is desirable to etch a deep trench to the GaAs substrate between the VCSEL and detector as we have demonstrated in previous integrated sensor designs [20].

The final processing step is to deposit the dielectric emission filter that will block backscattered VCSEL light from reaching the top of the detector, yet allow fluorescence light to pass through. The emission filter is patterned on the detector mesa using a bilayer liftoff process [33] (Fig. 2f), and deposited with electron-beam evaporation. The multilayer dielectric stack filter passes normal-incident fluorescence emission centered at 750nm with a bandwidth of 40nm. The filter is designed to reject at least six orders of magnitude of 675nm excitation light up to an acceptance angle of 30 degrees from normal. Because the emission filter is ~7µm thick, we developed a bilayer liftoff process using thick photoresists for a reliable liftoff of the emission filter film dielectric stack. The bilayer is composed of 7µm thick LOR30B (MicroChem Corp., Newton, MA) liftoff photoresist and 14µm thick AZ9260 photoresist (AZ Electronic Materials USA Corp., Somerville, NJ). Soft baking of the thick LOR layer on a hot plate with a slow temperature ramp (~2 hours) is necessary to prevent the formation of air bubbles.

The completed sensors are diced to include two sensor elements in each package, followed by the mounting of the sensors onto a miniature package, wire bonding to contact pads, and mounting of a collimation lens (NA = 0.55, Thorlabs Inc., Newton, NJ). The lens is anti-reflective (AR) coated in the NIR to minimize laser back reflection into the detector. In order to mitigate excitation light reaching the photodetector, the sensor package is designed to limit the angular acceptance of tissue-backscattered light. However, reflections from stray isotropic excitation light inside the package (e.g. spontaneous emission from the VCSEL) will be incident on the photodetector at large angles. Light blocking by the monolithically-integrated dielectric emission filter is angle-dependent and mostly transmitting at these high angles. Therefore, the sensors are packaged with an additional external miniature optical emission filter—including both absorption and interference components (hq750/40; Chroma Technology, Inc.)—bonded directly to the photodetector.

4. Optoelectronic device characterization

4.1 VCSEL and photodetector

We have achieved both reasonable laser output and extremely low dark current values in arrays of monolithically integrated sensor devices, using the fabrication steps described above. At room temperature, the VCSEL emits at 675nm (+/− 1nm) with FWHM linewidth <0.2nm
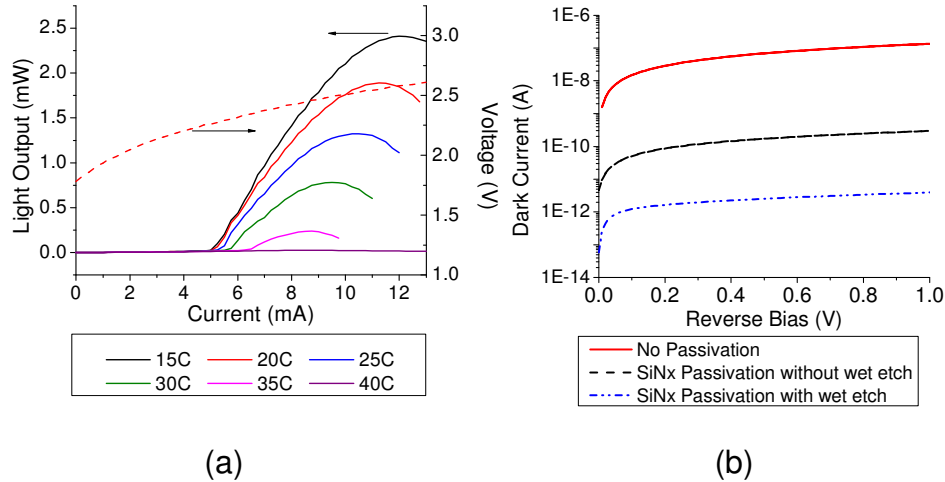
Fig. 3. (a) LIV Characteristics of the integrated VCSEL (device shown has a 12µm oxide aperture) and (b) demonstration of the reduced PIN photodetector dark current with sidewall cleaning and passivation

while achieving laser power values up to 2.0mW in transverse multi-mode operation (Fig. 3a). The adjacent photodetector generates less than 5.0pA dark current, when measured at reverse bias values up to 1V with internal quantum efficiencies η_{QE} greater than 75 percent.

VCSEL peak-output power values decrease with increasing operation temperature above RT, with lasing ceasing around 40°C. Because the devices are designed for implantable operation, we desire to improve the temperature performance to achieve stable lasing output at body temperatures (~37°C). We believe that a parasitic leakage current is causing additional heating near the VCSEL active region, contributing to the poor performance above 40°C and higher-than-expected 5-6mA laser threshold values. However, this leakage current can be easily reduced by reducing the oxide aperture diameter and/or employing an ion implant step for greater current confinement, a design modification we will employ in the next generation of devices. Other (not integrated) VCSEL devices employing these modifications and processed from the same epitaxy material exhibit the desired thermal performance.

Dark current in the PIN photodetector is dominated by carrier generation at the air/semiconductor interface. We thus employed techniques to clean and passivate the PIN photodetector sidewalls and were successful at reducing the dark current by four orders of magnitude (Fig. 3b). We prefer to use a plasma dry etch to define the detector layout geometry because a wet etch does not provide the required etch depth uniformity across the etched wafer for reliable stopping on the photodetector (and VCSEL) p-contact layer. However, the plasma-based dry etch process introduces electronic damage to the detector sidewalls in the form of surface defect/generation states. We found it beneficial to use the wet etch to etch-back the sidewalls while simultaneously etching the remainder of the top detector epitaxial layers above the AlGaAs etch-stop layer. The sidewalls are encapsulated in a silicon nitride passivation layer, and the devices show negligible increase in dark current over several months of testing.

4.2 Optical filtering

Minimizing the optical crosstalk between the VCSEL and photodetector components is critical for sensitive detection of fluorescence emission. Both stimulated and spontaneous VCSEL emissions contribute to the crosstalk, as summarized in Table 1. In general, stimulated excitation light will be incident on the top of the detectors, within a controllable angle of incidence (for example, by using an appropriate aperture size). Spontaneous emission

can be incident on the PIN active region from all directions (including the bottom) and in a large range of angles due to multiple reflections inside the package.

Table 1. Contributions to optical crosstalk in the integrated sensor

Spontaneous Emission	Stimulated Emission
Scattering from tissue volume	Scattering from tissue volume
Reflections from sensor package / collimation lens	Back-reflection from collimation lens
Lateral transmission into VCSEL structure below photodetector	

For this reason, we believe VCSELs to be superior to LEDs for this integrated sensor application. As mentioned earlier, we employed multiple design elements to mitigate crosstalk, using a thin film interference- based filter to primarily reduce back-reflected and backscattered and an absorption-based filter for blocking high-angle reflections from spontaneous emission. Metal blocking layers prevent light from being absorbed through the exposed sidewalls, and thus detected light must be incident from the filtered top side or through the epitaxial layers underneath.

We designed the nearest detector to each VCSEL pair to operate as an unfiltered reference detector to monitor laser intensity (via tissue backscattering). However, we underestimated crosstalk due to the lateral transmission of spontaneous emission from the VCSEL into the DBR layers below the photodetector. Because of the absence of metal blocking layers between the VCSEL active region and the adjacent detector, a large fraction of spontaneous emission is transmitted into DBR layers below the adjacent photodetector, and then guided towards the intrinsic absorption region of the photodetector. The light in this pathway couples surprisingly well, and we can use this to monitor the VCSEL spontaneous emission directly, from which stimulated output can be deduced [34]. We have not fully explored the utility of a reference-detector, and thus do not discuss those results here.

Figure 4 illustrates the effectiveness of the filtering techniques to blocking crosstalk between a VCSEL and the fluorescence photodetector. In these experiments, a 2x1 array of sensor elements are used with the first element reporting on excitation light (and serving as a reference detector), and the second as a fluorescence photodetector. Figure 4a shows the spectral sensitivity of the photodetector at NA = 0.4, overlaid with Cy5.5 emission spectra. Because of the interference filter, this window shifts towards the blue at higher incident angles, and is designed for suitable blocking up to thirty degrees from normal. We quantified the magnitude of excitation leakage through different filter configurations as a function of VCSEL drive current (Fig. 4b), as packaged for a fluorescence experiment.
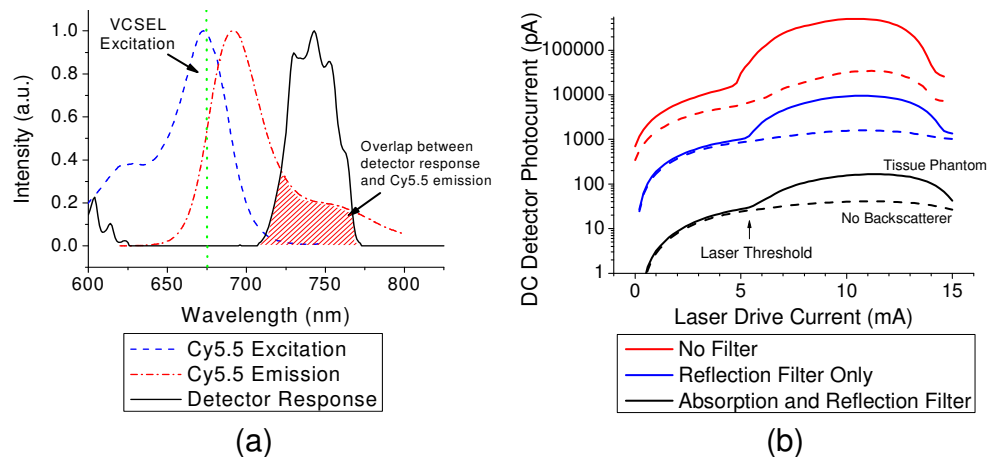
Fig. 4. (a) Integrated sensor excitation/emission spectra overlaid with Cy5.5 characteristics and (b) normalized crosstalk between VCSEL and detector under different filter configurations (the laser threshold varies slightly in the different configurations because each curve represents a different device)

Compared to an un-filtered detector, the combined interference/absorption filter rejects three orders of leaked excitation light in experimental conditions (using a tissue phantom). Note the large component of crosstalk due to spontaneous emission below laser threshold, where total emitted power is much lower compared to above threshold. Even though total optical emission power increases 100-1000x above threshold, crosstalk increases a mere 10x.

5. Fluorescence sensitivity

One determination of the performance of the integrated sensor is a measure of the smallest number of fluorescent molecules that can be sensed. We define this as "sensitivity," and such a measure is dependent upon the combined performance of the photodetector, excitation source, and filtering components. We measure the fluorescence sensitivity of the sensor in two conditions: 1) to concentrations of Cy5.5 in vitro under controlled conditions, and 2) to concentrations of Cy5.5 injected subcutaneously in a live, anesthetized nude (Nu/Nu) mouse.

5.1 In vitro sensitivity

We determine the in vitro sensitivity of the integrated sensor by measuring the fluorescence emission from aqueous dilutions of Cy5.5 in 100μL volumes. This allows us to determine the linear dynamic range of sensitivity, quantify the noise values, and determine the lowest concentration that can be reliably sensed in vitro. The sensor package, which includes an integrated collimation lens, was fixed below a clear-bottom plastic well (~7mm diameter) (Stripwell 1 x 8, Corning Inc.). Cy5.5-NHS (GE Healthcare/Amersham) was hydrolyzed in PBS to remove the reactive group, stored at −20C, and diluted at appropriate concentrations in PBS. After measuring control samples containing buffer solution without fluorophore, the well is emptied and Cy5.5 solutions are introduced incrementally from low to high concentration. The well is rinsed with buffer solution between consecutive concentrations to verify that the sensor signal returns to the initial background signal recorded during the control measurements. We utilize a lock-in technique to reduce the electrical noise in the system: the VCSEL is powered with a 1mA sinusoidal peak-to-peak current waveform at 23Hz overlaid on a 7mA current offset while the photodetector signal is recorded with a lock-in amplifier using a 300ms time constant.

Figure 5 shows that these sensors are able to detect Cy5.5 concentrations as low as 5nM in vitro. Sensor response is linear for over 3 orders of magnitude, limited at the top by dye quenching effects and not by the sensor performance, similar to our previous studies

[12,26,33]. Concentrations below 5nM cannot be reliably sensed since the detected photocurrent values vary due to changes in backscattered excitation light. Small perturbations in the position of the well containing the dye relative to the sensor as well as the laser output power fluctuations cause variations in the detected control signal on the order of 1 pA-RMS. However, within a measurement, the noise floor is measured to be 0.25 pA-RMS, equal to
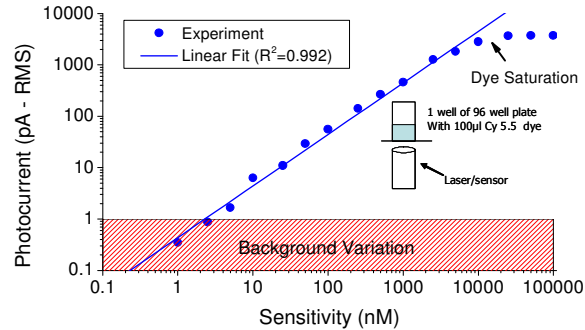

Fig. 5. Measured response of the integrated sensor to varying concentrations of Cy5.5 in PBS solution; Inset: schematic of the experiment

three standard deviations (3σ) of the mean signal sensed during the control measurements (N = 10). This implies that this sensor could likely detect Cy5.5 concentrations as low as 1nM using a better-controlled sample volume, such as in a microfluidic system. We note that the sensitivity, measured as a concentration (moles/liter) is strongly dependent on the volume illuminated by the VCSEL excitation source, and the sensor collection efficiency from that volume into the detector. A detailed quantitative analysis of these factors is described in our previous work [12,26]. We specifically targeted a large interrogation volume for in vivo tissue measurements. Greater sensitivity could be achieved by optimizing the collection efficiency of the detector to interrogate a much smaller volume. For our sensing geometry, the illuminated volume in the dye well is determined by the beam width of the VCSEL after the collimation lens (~2mm) and the dye depth (~3mm). This results in an excited dye solution volume of ~10µL, or 50 femtomole of excited dye molecules at the lowest measured sensitivity (5nM). To the best of our knowledge, this concentration sensitivity is comparable to the highest performing integrated fluorescence sensors at other wavelengths [27].

5.2 In vivo sensitivity

The sensitivity of the integrated sensor to in vivo fluorophore is determined by measuring fluorescence emission from subcutaneous injections of Cy5.5 dilutions in the dorsum of live, anesthetized, nude (Nu/Nu) mice. All animal studies were approved by the Institutional Administrative Panel on Laboratory Animal Care. Each mouse is anesthetized using 2-3% isofluorane, and we utilize two sensors in contact with the future injection sites on the left and right dorsum of the mouse to record a background measurement (Fig. 6a). The mouse then receives a 50µL subcutaneous injection of a Cy5.5 dilution in the right dorsum. The left dorsum is used as a control, with either no injection, or with an injection of buffer solution. The experiment is repeated for varying concentrations, with each concentration measured for at least 2 trials in different mice. Similar to the in vitro experiment, the fluorescence signal is determined by subtracting the background signal (due to backscattering and autofluorescence) from the measured photocurrent after injection. After measuring with the integrated sensor, the mouse is brought to a small animal CCD-based fluorescence imager (IVIS, Caliper Life Sciences, Hopkinton, MA) for comparison. We have verified using time sequential imaging that the detected fluorescence intensity does not change appreciably in the time elapsed between the sensor measurements and CCD imaging steps.

Figure 6b displays the response of the integrated sensor to the varying concentrations of subcutaneously injected Cy5.5 solution. The response is linear over two orders of magnitude,

with a detection limit of approximately 50nM. Similar to the discussion above for the in vitro sensitivity, and assuming a tissue penetration depth of ~2mm [26], a concentration of 50nM corresponds to 320 femtomole Cy5.5 dye molecules in the interrogated volume. Minimum detection in vivo is also limited by uncertainty due to background variation. For example, while collecting background data before injection, placement of the sensor in several locations around the control site causes the signal to vary by approximately 3pA-RMS. This higher variability, compared to the in vitro measurement, may be due to both variations in autofluorescence and excitation backscatter. The measurement is validated by comparing the sensor photocurrent to data collected with a CCD-based small animal imaging system. Figure 7a shows the maximum radiance observed from a region of interest enclosing the injection site plotted against the integrated sensor photocurrent. There is excellent correlation over the entire range of Cy5.5 concentrations, validating the performance of the miniature sensor. Figure 7b shows fluorescence images of two animals which have been separately injected with 25nM and 50nM Cy5.5 solutions, collected with a CCD-based small animal imaging system. The image of the 50nM animal shows a maximum radiance at the injection site approximately two times higher than the autofluorescence in the remainder of the animal. There is no contrast between the autofluorescence from the 25nM injection site and other sections of the mouse. The data shows that 675nm nude mouse autofluorescence in the Cy5.5 emission band is at the same magnitude as 25-50nM subcutaneous concentrations of Cy5.5.

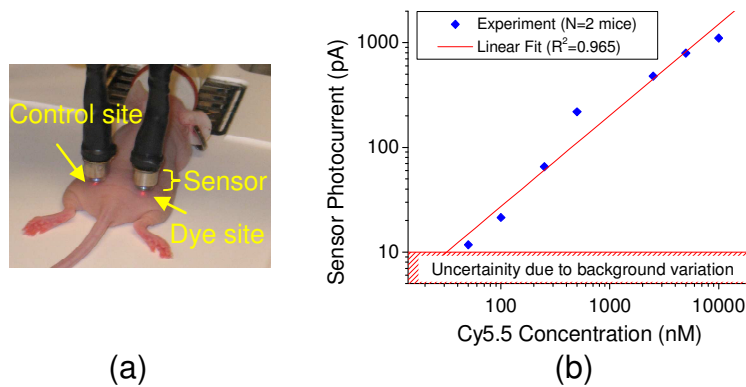
(a)   (b)

Fig. 6. (a) Photograph showing the sensor placement during an experiment in a living mouse to determine sensitivity and (b) experimental response of the sensor to varying concentrations of subcutaneously injected Cy5.5 in nude mice (N = 2 mice at each concentration)
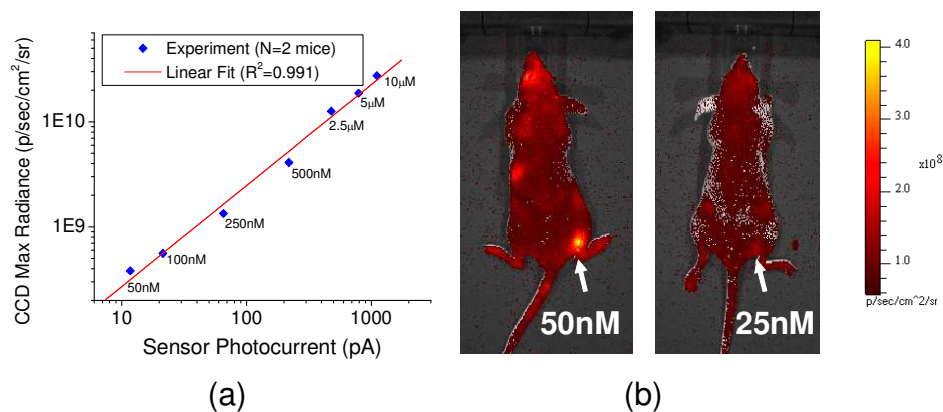

(a)   (b)

Fig. 7. (a) Comparison of the integrated sensor response to data from a CCD-based small animal fluorescence imager and (b) fluorescence images of mice injected with 50 and 25nM concentrations of Cy5.5

This agrees well with the 50nM autofluorescence limit reported by Sevick-Muraca and Rasmussen [25]. Importantly, we show that the integrated fluorescence sensor device is not limited by technological constraints, but instead by the autofluorescence of the animal subject in this application. Furthermore, this miniature sensor is designed to enable long-term interrogation of deep tissue by directly implanting it in close proximity to the target. Such a sensor provides the level of sensitivity as the large-format CCD-based fluorescence imagers utilized in numerous applications while providing better temporal resolution and opportunity for long-term continuous recording of fluorescence from freely-moving living subjects.

6. Conclusion

We have designed and fabricated an implantable, semiconductor-based sensor for in vivo fluorescence sensing in small animals. Similar to devices developed for lab-on-a-chip applications, the sensor is a monolithic integration of the optical components of a fluorescence imager, including a laser source, photodetector, and fluorescence emission filter. We have extended the sensor technology into far-red/visible wavelengths, which enables a commonly-used class of fluorescent probes and emerging fluorescent proteins, and discussed our design choices that optimize the device for sensing in living small animals. The sensor is sensitive to 5nM Cy5.5 in vitro and 50nM in nude mice, limited in vivo by the autofluorescence from the animal tissue, and not by the sensor technology. This miniature sensor thus provides the same sensitivity as large-format fluorescence imagers in this wavelength range. These sensors are promising to provide continuous, real-time molecular sensing that can enhance the basic understanding of molecular processes including tumor growth and drug treatment response all in live animals.

Future work includes implanting the sensor inside a live animal in order to evaluate stability and performance of the device over time periods from several hours to days. We also plan to further miniaturize the sensor package in order to make it less invasive to the animal. Since the present device relies on the electronic readout of a low-level current signal, we are in the process of incorporating components to amplify the sensor signal and thus reduce electrical noise. When completed, we hope to demonstrate real-time, continuous fluorescence sensing in freely-moving rodents.